Femtosecond coherent fields induced by many-particle correlations in transient four-wave mixing

W. Schäfer
Forschungszentrum Jülich, Höchstleistungsrechenzentrum, D-52425 Jülich, Germany

D. S. Kim
Department of Physics, Seoul National University, Seoul 151, Korea

J. Shah, T. C. Damen, J. E. Cunningham, and K. W. Goossen
AT&T Bell Laboratories, Holmdel, New Jersey 07733

L. N. Pfeiffer
AT&T Bell Laboratories, Murray Hill, New Jersey 07974

K. Köhler
Fraunhofer-Institut für angewandte Festkörperphysik, D-7800 Freiburg, Germany
(Received 20 March 1995; revised manuscript received 9 January 1996)

We present a unified microscopic approach to four-wave mixing (FWM) in semiconductors on an ultrashort time scale. The theory is valid for resonant excitation in the vicinity of the excitonic resonance and at low densities. The most important many-particle effects, i.e., static and dynamical exciton-exciton interaction as well as biexcitonic effects are incorporated. The internal fields resulting from these interaction processes give rise to pronounced many-particle effects in FWM signals. Our results explain the dependence of FWM signals on the polarization geometry, especially if biexcitons contribute. Time-resolved (TR) FWM experiments show that the diffraction of the interaction induced fields dominate the FWM signals completely. This dominance of the interaction induced field at low temperatures is true regardless of density, detuning, or polarization geometry. While spectrally resolved FWM (-FWM) shows biexcitonic or bound excitonic contributions under various experimental conditions, TR-FWM is always completely delayed, peaking roughly at the dephasing time after both beams passed through. [S0163-1829(96)00520-6]

I. INTRODUCTION

When a semiconductor or a semiconductor structure is excited by a short laser pulse, the induced polarization depends sensitively on interactions between elementary excitations in these systems. The Coulomb interaction between the excited charge carriers creates microscopic fields, which decay for long times exponentially, due to disspative processes like scattering with phonons, impurities, or lattice imperfections, or nondissipative scattering within the particle system. Excitation on an ultrashort time scale, i.e., if the pulse duration is short on the scale on which microscopic relaxation and dephasing processes take place, induces a complicated temporal evolution of the polarization, which determines the nonlinear response of the system.

Nonlinear optical transmission or absorption spectra reflect the time evolution of the system in the form of complicated modifications of the spectral line shape only. An experimental method allowing a more direct background-free approach to the study of interaction processes is four-wave mixing (FWM),[1,2] which has been proved in recent years as a powerful tool to investigate, in a direct manner, the coherent excitation of the system and the scattering processes which destroy this coherence. One form of this technique, the two-beam self-diffracted FWM, where the time-integrated signal (TI-FWM) is measured as a function of time delay T between the two pulses [compare Fig. 1(a)], has been widely used in GaAs and GaAs based quantum wells yielding much valuable information about interactions between excitons, bound excitons, biexcitons, Fermi edge singularities, free carriers, and phonons.[3–17]

Most of these experiments were analyzed using the well-known results for two-level systems,[18] which describe adequately weakly interacting systems such as gases or dilute solutions, only. In contrast, in solids, any interaction, which leads on the level of linear optics to the formation of quasiparticles, yields on the level of nonlinear optics an interaction between these quasiparticles. One particular example is the attractive exchange interaction between excited electron-hole pairs, which gives rise to excitonic bound states. Although the lowest exciton state together with the ground state realizes a two-level system within the framework of linear optics,[19] this model fails completely in nonlinear optics, as it neglects the interaction between the excitons. For excitation in the vicinity of the excitonic resonance, nonlinear optical properties are dominated by these interaction effects.[20–26,29–33]

Whereas first experimental data[20–26] demonstrated the importance of interaction effects unambiguously, their interpretation and analysis performed within the framework of the semiconductor Bloch equations (SBE's),[27–29] was restricted only to the effect of the static exciton-exciton interaction.[29–33] In this approximation, i.e., on the Hartree-Fock level, the induced field is proportional to the convolution in $\mathbf{k}$ space of the bare Coulomb potential with the polarization. The corresponding renormalization of the bare

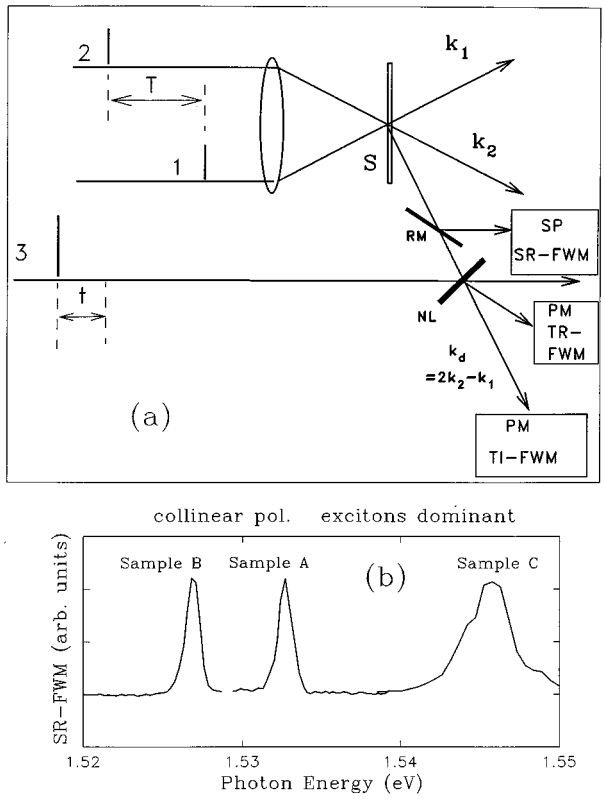

FIG. 1. (a) Schematics for TI-, TR-, and SR-FWM experiments. In TR-FWM, the diffracted signal in direction of k_d is upconverted in a nonlinear crystal (NL) with a third beam. The time delay (t) thus introduced acts as a real time, so that the time evolution of the FWM signal at a fixed time delay (T) can be probed. S, SP, RM, and PM denote sample, spectrometer, removable mirror, and photomultiplier tube, respectively. (b) SR-FWM at low densities in the collinearly polarized geometry from samples A, B, and C.

Rabi-frequency gives rise to an interaction induced signal, which in TI-FWM is responsible for a contribution at negative time delays,[20–23] which can also result from biexcitonic correlations.[7,16]

An even more pronounced consequence of the exciton-exciton interaction shows up in time-resolved FWM (TR-FWM) signals. The usual free polarization decay, expected from a two-level description, is transformed into a nonmonotonous time evolution of the TR-FWM signal. If the pulse duration is short in comparison with the macroscopic dephasing time T_2, the signal continues to increase after both beams passed through and peaks roughly at T_2, independent of the delay between the pulses.[20,24,29,33] Considering more rapid dephasing rates, the decay of the signal becomes nearly exponential. Due to the interaction induced signal, however, the decay is substantially slower than the intrinsic dephasing time, which is obtained from TI-FWM signals.[26] This behavior is well described qualitatively by the SBE's.

It is, however, an easy task to show that any kind of interaction, regardless of its microscopic origin, can lead to such a nonmonotonous behavior of the TR-FWM signal. Even, the coupling of the excitation fields to the polarization via Maxwell equations can yield similar effects in TR-FWM signals, as well as a contribution for negative time delay in TI-FWM signals. This can be easily understood. As the electromagnetic fields result, together with appropriate boundary conditions from the spatial and temporal convolution of the transverse photon Green's function with the polarization, this coupling yields a scattering of the polarization off the induced transient density grating, rather than scattering of external fields themselves. Formally, this mechanism leads also to the occurrence of interaction induced signals and can be compared with the case of the static exciton-exciton interaction. The role of the Coulomb interaction, however, is taken over by the transverse photon Green's function. The resulting propagation effects increase with an increasing thickness of samples[34–41] and lead for excitation in the excitonic resonance to pronounced polariton effects.[34–36,40,41] In particular, if there are large differences between the absorption in different regions of the spectrum, which contribute to the signal, the temporal evolution of FWM signals depends crucially on the propagation length.[39] Genuine information about many-particle effects can thus be obtained from FWM signal from thin samples, only. Otherwise, propagation effects should be carefully taken into account.

Neither static exciton-exciton interaction nor propagation effects, however, can explain the dependence of FWM signals on the polarization of the incident laser fields. It was the investigation of these dependencies[42–49] which demonstrated that the SBE approach fails to explain details of the experimental findings. This is not surprising at all, as the shortcomings of the Hartree-Fock approximation are well known from the quasistationary description of highly excited semiconductors.[50] Screening in its various forms, as well as correlation effects, are missing in the SBE approach. Consequently, no influence of the excited pairs on the dephasing processes is present. Concerning the FWM signals, this neglection is especially unphysical. Even in lowest order in the laser fields, i.e., on the $\chi^{(3)}$ level, any interaction process between excited charge carriers acts as a source of the diffracted polarization, in addition to the contributions already present in the SBE approach. These source contributions have been classified as excitation induced dephasing.[43–46] To avoid confusion, we note that on a $\chi^{(3)}$ level, however, the decay of the FWM signal is not changed by these processes. In the lowest order, this occurs on a $\chi^{(5)}$ level. Details of excitation induced dephasing effects depend crucially on the excitation conditions and the theoretical description should take this dependence into account.

There are at least two ways which lead, within the restrictions of the usual simple model of the material system, to a quantitative theory of FWM in semiconductors. The first is based on the nonequilibrium Green's-function technique, which has been applied to various problems of nonlinear optics in recent years (for a recent review compare Ref. 49 and references therein). A standard approximation in this approach is the second-order Born approximation for the scattering self-energies, which is correct up to the second order in the Coulomb interaction. For the case of continuum excitation, where scattering processes between free-carriers dominate, this approximation seems to be well justified. In the vicinity of the excitonic resonance, scattering takes place between highly correlated electron-hole pairs. A consistent treatment of these correlations has to take the Coulomb interaction in arbitrary order into account. Already, on the $\chi^{(3)}$ level, this requires the solution of the quantum-mechanical three-body and four-body problems, not only for the ground

state, but also for all excited states.

An approach, which is best suited to derive the corresponding equations of motion, is the $\chi^{(3)}$ formalism.[51–53] The latter is based on the statement that any mutual interaction between electrons and holes in a semiconductor results from an optical excitation by external fields. This allows us to classify correlation functions of a given order, with respect to the power of the field, and yields a systematic truncation scheme of the many-particle problem at any given order in the field. As long as perturbation theory is valid and physically meaningful, this formalism represents the most rigorous approach to semiconductor optics in the coherent regime. A corresponding theory is worked out in Sec. II, where we apply the truncation scheme in the coherent limit different from Refs. 51–53, and derive a closed system of equations, which determines nonlinear optical properties.

From the general results, we derive a coupled set of few level equations, which qualitatively explain most experimental features for excitation in the vicinity of the excitonic or biexcitonic resonance. In addition to the static exciton-exciton interaction, our description includes excitation-induced dephasing, due to exciton-exciton scattering, as well as biexcitonic bound states, which have been intensively investigated during the past two decades (compare, e.g., Refs. 54–57) and are still a subject of current interest.[13–17,58–60] The incorporation of dissipative processes, using the technique applied in Refs. 51, 53, is straightforward, but beyond the scope of the present paper. The derived model represents under various respects a generalization of the so-called local-field model, introduced phenomenologically in Refs. 20, 26 and derived from the SBE's in Ref. 61. Furthermore, our results allow us to value purely phenomenological approaches proposed in.[17,62–64] Numerical results, which illustrate the predictions of our model, are discussed in Sec. III.

In the experimental part of this paper, we show that for various experimental conditions, TR-FWM signals are dominated by interaction induced fields. The microscopic origin of these fields can be revealed by considering the corresponding spectrally resolved (SR-FWM) signals. We present TR-FWM studies at different detunings, densities, and temperatures on two high quality GaAs quantum well samples *A* and *B* [compare Fig. 1(b)]. Both collinearly and cross linearly polarized geometries are used. As a function of density or detunings, TR-FWM at low temperatures is always dominated by an interaction induced signal, in the wide range from 3×10^{10} down to 3×10^{8} cm^{-2}, at detunings ranging from from -8 to $+4$ meV, from the heavy-hole (hh) resonance and for both polarizations. A typical example of TR-FWM signals is shown in Fig. 2(a).

SR-FWM shows [compare Fig. 2(b)] that the microscopic origin of the induced fields can be traced back, depending on the sample and the polarization geometry, to excitons, biexcitons, or bound excitons. We show that SR-FWM exhibits sharp peaks, which are consistent with the broad, delayed FWM signals in time domain. In the cross-linear polarization, the spectrum of sample *A* is dominated by bound excitons, whereas in sample *B* there is a strong biexcitonic contribution. Our results unambiguously demonstrate that the dominance of the diffraction of interaction induced fields is an intrinsic property. It should be emphasized that this unambiguous demonstration of dominance of interaction induced fields in FWM from excitons, biexcitons, or bound excitons was possible, only because our pulse widths ($\tau = 100$–200 fs) are always shorter than the dephasing times (200 fs–1.5 ps) under our experimental conditions.

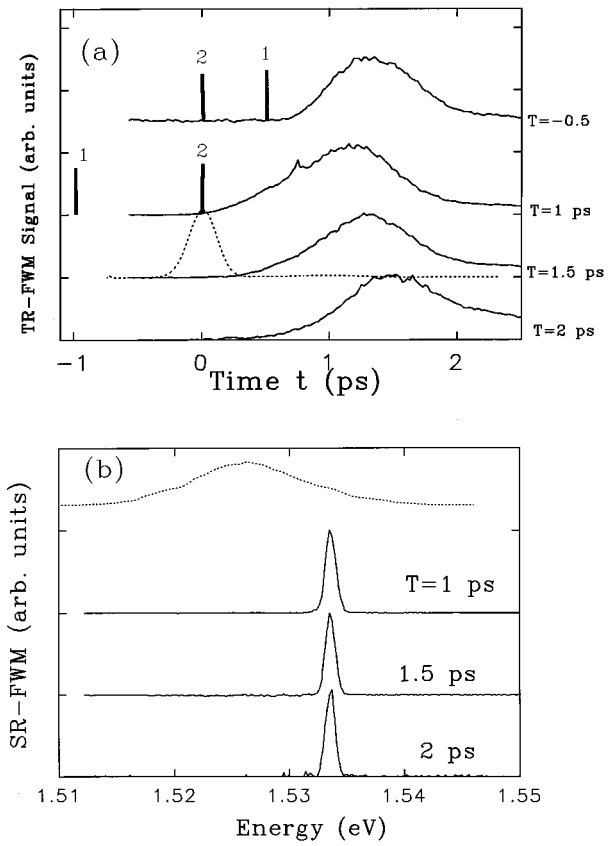

FIG. 2. TR-FWM from sample *A* at 10 K at various time delays at a detuning of -4 meV from the hh, obtained with collinearly polarized beams. The positions of beams 1 and 2 are indicated as thick lines for $T=-0.5$ ps and 1 ps. The time delays are, from top to bottom, 0.5, 1, 1.5, and 2 ps. Densities are estimated to be 10^{10} cm^{-2}. The transmitted pulse shape obtained by upconversion is represented by broken lines. (b) SR-FWM at time delays 1, 1.5, and 2 ps. The broken line at the top shows the laser spectrum.

In Sec. IV, we describe the samples and some of the experimental details. We have carefully checked that pulse distortion effects are minimal and thus propagation effects may be neglected. TR- and SR-FWM, which result from samples *A* and *B*, are discussed in Sec. V for the collinearly polarized geometry. In this configuration, excitons dominate FWM. The case of two cross linearly polarized beams is discussed in Sec. V. Again TR-FWM results are dominated by a delayed signal, whereas SR-FWM shows strong biexcitonic or bound excitonic contributions. Finally, the case of inhomogeneously broadened transitions is studied on sample *C* [compare Fig. 1(b)] in Sec. VII. Due to inhomogeneous broadening, the interaction induced signal is reduced and one obtains the clear signature of a photon echo. A summary and conclusions are drawn in Sec. VIII.

II. $\chi^{(3)}$ THEORY OF FOUR WAVE MIXING IN SEMICONDUCTORS IN THE COHERENT LIMIT

The variety of theoretical approaches, which have been proposed in recent years in order to analyze and explain

FWM signals, has led to some confusion in the literature. In the low-density limit, there are three basic physical ingredients, which can be classified as static exciton-exciton interaction, excitation-induced dephasing, and biexcitonic correlations. A special treatment of the static interaction effects in the SBE's for the case of resonant excitation of the lowest exciton state has been called the local-field model.[20,26,61] Excitation-induced dephasing is present in any FWM scenario and acts as an additional source of the FWM signal. Microscopically it may result from scattering between free carriers,[46] as well as from scattering between excitons.[19,43–45] A remarkable feature of these contributions is the property that they can be partially switched off by using certain polarization geometries. This leads to a pronounced dependence of FWM signals on the polarization geometry chosen. The third effect is the occurrence of bound biexciton states, which becomes important if the binding energy and the oscillator strength of this many-particle resonance are sufficiently large to be separated from the excitonic resonance. Apart from CuCl, biexcitons have been observed also in several II–VI bulk semiconductors.[56] Due to quantum-confinement effects in quantum wells, the binding energy and oscillator strength of biexcitons is considerably increased in comparison with bulk semiconductors. This has allowed the observation of biexcitonic features also in GaAs-based quantum wells.[13–17,59,60,64] In the following, we will derive a model, which yields at low densities a unified picture of FWM in semiconductors.

We start our discussion with the off-diagonal elements of the one-particle density matrix, which determine the optical polarization and which in terms of electron and hole Fermi operators $e_{\mathbf{k}}^{\dagger}$ and $h_{\mathbf{k}}^{\dagger}$, respectively, is given by

$$P_{\mathbf{k}}^{eh}=\langle e_{\mathbf{k}}^{\dagger}h_{\mathbf{k}}^{\dagger}\rangle, \tag{2.1}$$

where e and h indices denote electron and hole bands of an arbitrary multiband model of a semiconductor which will be specified later. Using the common many-particle Hamiltonian, including the coupling to external fields within the dipole approximation (compare, e.g., Ref. 49), the equation of motion of the polarization is given by

$$\begin{aligned}\left(-i\hbar\frac{\partial}{\partial t}-i\gamma-\varepsilon_{\mathbf{k}}^{e}-\varepsilon_{\mathbf{k}}^{h}\right)P_{\mathbf{k}}^{eh}+\sum_{\mathbf{q}}\nu_{\mathbf{k}-\mathbf{q}}P_{\mathbf{q}}^{eh}&\\ =\boldsymbol{\mu}^{eh}\mathbf{E}-\sum_{e'}\boldsymbol{\mu}^{e'h}\mathbf{E}f_{\mathbf{k}}^{ee'}-\sum_{h'}\boldsymbol{\mu}^{eh'}\mathbf{E}f_{\mathbf{k}}^{hh'}&\\ +\sum_{\mathbf{q}\mathbf{k}'e'}\nu_{\mathbf{q}}\{\langle e_{\mathbf{k}}^{\dagger}e'^{\dagger}_{\mathbf{k}'}h_{\mathbf{k}-\mathbf{q}}^{\dagger}e'_{\mathbf{k}'+\mathbf{q}}\rangle&\\ -\langle e_{\mathbf{k}+\mathbf{q}}^{\dagger}e'^{\dagger}_{\mathbf{k}'}h_{\mathbf{k}}^{\dagger}e'_{\mathbf{k}'+\mathbf{q}}\rangle\}&\\ +\sum_{\mathbf{q}\mathbf{k}'h'}\nu_{\mathbf{q}}\{\langle e_{\mathbf{k}+\mathbf{q}}^{\dagger}h'^{\dagger}_{\mathbf{k}'+\mathbf{q}}h_{\mathbf{k}}^{\dagger}h'_{\mathbf{k}'}\rangle&\\ -\langle e_{\mathbf{k}}^{\dagger}h'^{\dagger}_{\mathbf{k}'+\mathbf{q}}h_{\mathbf{k}-\mathbf{q}}^{\dagger}h'_{\mathbf{k}'}\rangle\}.&\end{aligned} \tag{2.2}$$

We now consider the coherent limit at low densities, in which dissipative, i.e., dephasing effects resulting, e.g., from scattering with phonons are negligible. For practical applications, it is sufficient to assume that the dephasing rate γ is small compared with the inverse duration of the pulse. In this limit, the Rabi vector is approximately conserved, i.e., the one-particle distribution, e.g., $f^{hh'}$ can be expressed by

$$f_{\mathbf{k}}^{h'h}=\langle h'^{\dagger}_{\mathbf{k}}h_{\mathbf{k}}\rangle=\sum_{e'}(P_{\mathbf{k}}^{e'h'})^{*}P_{\mathbf{k}}^{e'h}+O(E^{5}), \tag{2.3}$$

and similarly for the electron distribution. In the same limit the four-point functions in (2.2) can be replaced according to the $\chi^{(3)}$ decoupling scheme, which yields,[51,53] e.g.,

$$\begin{aligned}\langle e_{\mathbf{k}}^{\dagger}h'^{\dagger}_{\mathbf{k}'+\mathbf{q}}h_{\mathbf{k}-\mathbf{q}}^{\dagger}h'_{\mathbf{k}'}\rangle=\sum_{e'\mathbf{k}''}\langle e_{\mathbf{k}}^{\dagger}h'^{\dagger}_{\mathbf{k}'+\mathbf{q}}h_{\mathbf{k}-\mathbf{q}}^{\dagger}e'^{\dagger}_{\mathbf{k}''}\rangle\langle e'_{\mathbf{k}''}h'_{\mathbf{k}'}\rangle&\\ +O(E^{5}).&\end{aligned} \tag{2.4}$$

With these ingredients, we obtain from (2.2)

$$\begin{aligned}\left(-i\hbar\frac{\partial}{\partial t}-i\gamma-\varepsilon_{\mathbf{k}}^{e}-\varepsilon_{\mathbf{k}}^{h}\right)P_{\mathbf{k}}^{eh}+\sum_{\mathbf{q}}\nu_{\mathbf{k}-\mathbf{q}}P_{\mathbf{q}}^{eh}&\\ =\boldsymbol{\mu}^{eh}\mathbf{E}-\sum_{e'h'}(\boldsymbol{\mu}^{e'h}\mathbf{E}P_{\mathbf{k}}^{eh'}(P_{\mathbf{k}}^{e'h'})^{*}+\boldsymbol{\mu}^{eh'}\mathbf{E}(P_{\mathbf{k}}^{e'h'})^{*}P_{\mathbf{k}}^{e'h})&\\ +\sum_{\mathbf{q}e'h'}\nu_{\mathbf{k}-\mathbf{q}}[P_{\mathbf{q}}^{eh'}(P_{\mathbf{k}}^{e'h'})^{*}P_{\mathbf{k}}^{e'h}+P_{\mathbf{k}}^{eh'}(P_{\mathbf{k}}^{e'h'})^{*}P_{\mathbf{q}}^{e'h}&\\ -P_{\mathbf{q}}^{eh'}(P_{\mathbf{q}}^{e'h'})^{*}P_{\mathbf{k}}^{e'h}-P_{\mathbf{k}}^{eh'}(P_{\mathbf{q}}^{e'h'})^{*}P_{\mathbf{q}}^{e'h}]&\\ +\sum_{\mathbf{k}'\mathbf{q}e'h'}\nu_{\mathbf{q}}(P_{\mathbf{k}'}^{e'h'})^{*}(B_{\mathbf{k}+\mathbf{q},\mathbf{k}'+\mathbf{q},\mathbf{k}',\mathbf{k}}^{eh'e'h}-B_{\mathbf{k}+\mathbf{q},\mathbf{k}',\mathbf{k}'-\mathbf{q},\mathbf{k}}^{eh'e'h}&\\ +B_{\mathbf{k},\mathbf{k}',\mathbf{k}'-\mathbf{q},\mathbf{k}-\mathbf{q}}^{eh'e'h}-B_{\mathbf{k},\mathbf{k}',\mathbf{k}'+\mathbf{q},\mathbf{k}-\mathbf{q}}^{eh'e'h}).&\end{aligned} \tag{2.5}$$

The first group of contributions on the right-hand side of (2.5) describes the phase-space filling, whereas the second group corresponds to the static Coulomb interaction, within the approximation of Eq. (2.3). In the third group, which takes the correlation effects beyond the Hartree-Fock approximation into account, we have introduced a four-point correlation function

$$\begin{aligned}B_{\mathbf{k}+\mathbf{q},\mathbf{k}'+\mathbf{q},\mathbf{k}',\mathbf{k}}^{eh'e'h}=\langle e_{\mathbf{k}+\mathbf{q}}^{\dagger}h'^{\dagger}_{\mathbf{k}'+\mathbf{q}}e'^{\dagger}_{\mathbf{k}'}h_{\mathbf{k}}^{\dagger}\rangle-\langle e_{\mathbf{k}+\mathbf{q}}^{\dagger}h'^{\dagger}_{\mathbf{k}'+\mathbf{q}}\rangle&\\ \times\langle e'^{\dagger}_{\mathbf{k}'}h_{\mathbf{k}}^{\dagger}\rangle-\langle e_{\mathbf{k}+\mathbf{q}}^{\dagger}h_{\mathbf{k}}^{\dagger}\rangle\langle e'^{\dagger}_{\mathbf{k}'}h'^{\dagger}_{\mathbf{k}+\mathbf{q}}\rangle,&\end{aligned} \tag{2.6}$$

instead of the bare four-point function [first term on the right-hand side of (2.6)]. This yields the explicit occurrence of the Hartree-Fock contributions in (2.5). As will be shown later, this kind of decoupling introduces explicitly excitonic correlations, which correspond to biexcitonic scattering states and lead to excitation induced dephasing.

An even more general correlation function, avoiding the approximation of (2.3), has been discussed only recently in Ref. 53. The correlation function (2.6) obeys the equation of motion,

$$\left(-i\frac{\partial}{\partial t}-\varepsilon^{e}_{\mathbf{k}+\mathbf{q}}-\varepsilon^{h'}_{\mathbf{k}'+\mathbf{q}}-\varepsilon^{e'}_{\mathbf{k}'}-\varepsilon^{h}_{\mathbf{k}}\right)B^{eh'e'h}_{\mathbf{k}+\mathbf{q},\mathbf{k}'+\mathbf{q},\mathbf{k}',\mathbf{k}}$$
$$-\sum_{\mathbf{q}'}\nu_{\mathbf{q}'}[B^{eh'e'h}_{\mathbf{k}+\mathbf{q}+\mathbf{q}',\mathbf{k}'+\mathbf{q},\mathbf{k}'-\mathbf{q}',\mathbf{k}}+B^{eh'e'h}_{\mathbf{k}+\mathbf{q},\mathbf{k}'+\mathbf{q}-\mathbf{q}',\mathbf{k}',\mathbf{k}+\mathbf{q}'}-B^{eh'e'h}_{\mathbf{k}+\mathbf{q}+\mathbf{q}',\mathbf{k}'+\mathbf{q}-\mathbf{q}',\mathbf{k}',\mathbf{k}}-B^{eh'e'h}_{\mathbf{k}+\mathbf{q},\mathbf{k}'+\mathbf{q},\mathbf{k}'+\mathbf{q}',\mathbf{k}+\mathbf{q}'}-B^{eh'e'h}_{\mathbf{k}+\mathbf{q}+\mathbf{q}',\mathbf{k}'+\mathbf{q},\mathbf{k}',\mathbf{k}+\mathbf{q}'}-B^{eh'e'h}_{\mathbf{k}+\mathbf{q},\mathbf{k}'+\mathbf{q}-\mathbf{q}',\mathbf{k}'-\mathbf{q}',\mathbf{k}}]$$
$$=-\nu_{\mathbf{q}}(P^{eh}_{\mathbf{k}}-P^{eh}_{\mathbf{k}+\mathbf{q}})(P^{e'h'}_{\mathbf{k}'+\mathbf{q}}-P^{e'h'}_{\mathbf{k}'})+\nu_{\mathbf{k}-\mathbf{k}'}(P^{eh'}_{\mathbf{k}'+\mathbf{q}}-P^{eh'}_{\mathbf{k}+\mathbf{q}})(P^{e'h}_{\mathbf{k}}-P^{e'h}_{\mathbf{k}'}). \quad (2.7)$$

Whereas the right-hand side of (2.7) describes the usual biexciton problem[55] in **k**-space representation, the inhomogeneity corresponds to the low-density limit of the random phase approximation contributions to correlation (first term) and the corresponding exchange-type contributions. In the case of continuum excitation, one can neglect the Coulomb interaction on the left-hand side. The formal solution of the corresponding equation combined with (2.5) is nothing but the low-density contribution to the second-order Born approximation for diagonal and off-diagonal elements of the self-energy (compare, e.g., Ref. 46), within the approximation of (2.3). In the opposite limit when only a spectrally narrow range in the vicinity or below the excitonic ground state is excited, the problem can be considerably simplified by expanding (2.5) and (2.7) in terms of excitonic and biexcitonic eigenfunctions.

The polarization in (2.5) can be expanded according to

$$P^{eh}_{\mathbf{k}}=\sum_{n}P_n\phi_n(\mathbf{k}). \quad (2.8)$$

Further, we make use of the expansion

$$B^{eh'e'h}_{\mathbf{k}+\mathbf{q},\mathbf{k}'+\mathbf{q},\mathbf{k}',\mathbf{k}}=\sum_{nm}\phi_{n\mathbf{q}}(\mathbf{k}+\beta\mathbf{q})B^{eh'e'h}_{nm\mathbf{q}}\phi_{n\mathbf{q}}(\mathbf{k}'+\alpha\mathbf{q}), \quad (2.9)$$

with $\alpha=m_e/(m_e+m_h)$, $\beta=m_h/(m_e+m_h)$, and $\phi_{n\mathbf{q}}$ are excitonic eigenfunctions with finite center-of-mass momentum $\mathbf{q}$. If we assume resonant excitation conditions, in which the lowest excitonic bound state with eigenvalue ε_0, is excited, P_n can be replaced by the $1s$ contribution to the polarization $P^{eh}_0=P^{eh}$. With these assumptions we obtain, from (2.5),

$$\left(-i\frac{\partial}{\partial t}-i\gamma-\varepsilon_0\right)P^{eh}$$
$$=-\boldsymbol{\mu}^{eh}\mathbf{E}\tilde{\phi}_0(0)+\sum_{e'h'}[\boldsymbol{\mu}^{e'h}\mathbf{E}b^{eh'e'h'}P^{eh'}(P^{e'h'})^*+\boldsymbol{\mu}^{eh'}\mathbf{E}b^{e'he'h'}P^{eh'}(P^{e'h'})^*+V_{\mathbf{st}}P^{eh'}(P^{e'h'})^*P^{e'h}]+\left\{\frac{\partial}{\partial t}P^{eh}\right\}\Big|_{\mathrm{corr}}, \quad (2.10)$$

where the correlation part, which results from the four-point function in (2.5), is given by

$$\left\{\frac{\partial}{\partial t}P^{eh}\right\}\Big|_{\mathrm{corr}}=\sum_{\mathbf{q}nme'h'}\nu_{\mathbf{q}}(P^{e'h'})^*B^{eh'e'h}_{nm\mathbf{q}}M^{e'h'}_{0n,\mathbf{q}}M^{eh}_{0m,-\mathbf{q}}. \quad (2.11)$$

Apart from the correlation contribution, Eq. (2.10) represents the multiband version of the nonlinear Schrödinger equation discussed in Refs. 20, 26, 61. The various quantities are defined as follows. The Pauli-blocking parameter b is given by

$$b^{eh'e'h'}=\sum_{\mathbf{k}}\phi^{eh}_0(\mathbf{k})\phi^{eh'}_0(\mathbf{k})\phi^{e'h'}_0(\mathbf{k}). \quad (2.12)$$

The static interaction parameter V_{st} results from

$$V_{\mathrm{st}}=\sum_{\mathbf{kq}}\nu_{\mathbf{k}-\mathbf{q}}\{\phi^{eh}_0(\mathbf{k})[\phi^{e'h'}_0(\mathbf{k})-\phi^{e'h'}_0(\mathbf{q})]\times[\phi^{eh'}_0(\mathbf{q})\phi^{e'h}_0(\mathbf{k})+\phi^{eh'}_0(\mathbf{k})\phi^{e'h}_0(\mathbf{q})]\}. \quad (2.13)$$

The excitonic transition matrix elements are defined as

$$M^{eh}_{0n\mathbf{q}}=\sum_{\mathbf{k}}\phi^{eh}_0(\mathbf{k})[\phi^{eh}_n(\mathbf{k}-\alpha\mathbf{q})-\phi^{eh}_n(\mathbf{k}+\beta\mathbf{q})]. \quad (2.14)$$

Finally, the biexcitonic correlation function has to be calculated from

$$\left(-i\frac{\partial}{\partial t}-\varepsilon^{eh}_{n\mathbf{q}}-\varepsilon^{e'h}_{m\mathbf{q}}\right)B^{eh'e'h}_{nm\mathbf{q}}$$
$$=-\nu_{\mathbf{q}}M^{e'h'}_{0n,\mathbf{q}}{}^{*}M^{eh}_{0m,-\mathbf{q}}{}^{*}P^{eh}P^{e'h'}+\sum_{\mathbf{kk}'}\nu_{\mathbf{k}-\mathbf{k}'}\phi^{eh}_{n\mathbf{q}}{}^{*}(\mathbf{k}+\alpha\mathbf{q})\times\phi^{e'h'}_{m\mathbf{q}}{}^{*}(\mathbf{k}'+\beta\mathbf{q})[\phi^{eh'}_0(\mathbf{k}'+\mathbf{q})-\phi^{eh'}_0(\mathbf{k}+\mathbf{q})]\times[\phi^{e'h}_0(\mathbf{k})-\phi^{e'h}_0(\mathbf{k}')]P^{eh'}P^{e'h}$$
$$+\sum_{\mathbf{q}'\mathbf{kk}'}\nu_{\mathbf{q}'}\phi^{eh}_{n\mathbf{q}}{}^{*}(\mathbf{k}+\alpha\mathbf{q})\phi^{e'h'}_{m\mathbf{q}}{}^{*}(\mathbf{k}'+\beta\mathbf{q})\times(\zeta_{\mathbf{k}+\mathbf{q}+\mathbf{q}',\mathbf{k}'+\mathbf{q},\mathbf{k}'-\mathbf{q}',\mathbf{k}}+\zeta_{\mathbf{k}+\mathbf{q},\mathbf{k}'+\mathbf{q}-\mathbf{q}',\mathbf{k}',\mathbf{k}+\mathbf{q}'}-\zeta_{\mathbf{k}+\mathbf{q}+\mathbf{q}',\mathbf{k}'+\mathbf{q}-\mathbf{q}',\mathbf{k}',\mathbf{k}}-\zeta_{\mathbf{k}+\mathbf{q},\mathbf{k}'+\mathbf{q},\mathbf{k}'+\mathbf{q}',\mathbf{k}+\mathbf{q}'})B^{eh'e'h}, \quad (2.15)$$

where $\varepsilon_{n\mathbf{q}}$ are excitonic eigenvalues in the states $\phi_{n\mathbf{q}}$ and ζ denotes the wave function of the bound biexciton state. All higher biexciton states, which occur, in principle, also in the last contribution on the right-hand side of (2.15) are neglected. This is a physically meaningful approximation, since all contributions up to second order in the Coulomb potential are treated explicitely, Thus, the biexcitonic continuum contributions, i.e., the dynamical interaction of free pairs of excitons are approximately taken into account, as well as the static Coulomb-interaction between excitons. The polarization of the biexcitonic bound state B, with energy ε_B, results from the expansion of (2.7), in terms of biexcitonic eigenstates as

$$\left(-i\frac{\partial}{\partial t}-\varepsilon_B\right)B^{eh'e'h}=c_B P^{eh}P^{e'h'}\delta_{h'\tilde{h}}\delta_{e'\tilde{e}}, \quad (2.16)$$

where $\tilde{e}(\tilde{h})$ denote the band with the opposite spin of the band $e(h)$ and c_B is defined as

$$c_B=\sum_{\mathbf{k}\mathbf{k}'\mathbf{q}}\zeta^*_{\mathbf{k}+\mathbf{q},\mathbf{k}'+\mathbf{q},\mathbf{k}'}\nu_{\mathbf{q}}[\phi_0^{eh}(\mathbf{k})-\phi_0^{eh}(\mathbf{k}+\mathbf{q})]\times[\phi_0^{e'h'}(\mathbf{k}'+\mathbf{q})-\phi_0^{e'h'}(\mathbf{k}')]. \quad (2.17)$$

As the bound state is present only for the pairing of opposite spins, the exchange-type contributions, proportional to $P^{eh'}P^{e'h}$, do not occur in the inhomogeneity of (2.16).

The system of equations derived up to now, could be treated numerically. In order to come into contact with the few level descriptions, we solve Eq. (2.15) within the rotating wave approximation, assume off-resonant excitation conditions, and perform the usual Markovian approximation. Inserting the corresponding result into (2.11), the correlation contribution takes the form

$$\left\{\frac{\partial}{\partial t}P^{eh}\right\}\Big|_{\text{corr}}=\sum_{e'h'}V_s(P^{e'h'})^*P^{e'h'}P^{eh}-V_{\text{exc}}(P^{e'h'})^*P^{eh'}P^{e'h}+V_B\tilde{B}^{eh'e'h}(P^{e'h'})^*\delta_{h'\tilde{h}}\delta_{e'\tilde{e}}, \quad (2.18)$$

where we have set $B=c_B\tilde{B}$.

The lengthy definitions of the parameters V_s describing excitonic screening, V_{exc} corresponding exchange processes, and V_B measuring the strength of exciton-biexciton interaction are obvious from (2.11), (2.14), and (2.17) and will not be given, explicitly. It should, however, be noted that all parameters apart from the static interaction parameter depend sensitively on the excitation conditions. Although the microscopic definition of these parameters is rather complicated and their calculation is beyond the scope of the present paper, the structure of the resulting set of coupled equations (2.10) and (2.16) is rather simple. Neglecting the biexcitonic correlation, it could be used to rediscover the selection rules for the diffracted signal that have been worked out e.g., in Ref. 48.

III. A GENERALIZED NONLINEAR SCHRÖDINGER EQUATION AND NUMERICAL SOLUTIONS

In order to investigate the predictions of the model derived in the last section, we specify the band indices for a zinc-blende semiconductor. The hole bands consist of $|-3/2h\rangle$, $|-1/2h\rangle$, $|1/2h\rangle$, and $|3/2h\rangle$ states, whereas electrons are in spin states $|-1/2e\rangle$ and $|1/2e\rangle$. Due to the optical selection rules, we have two separate subspaces of spin states, which cannot be coupled optically. They are, however, coupled by the excitonic screening contributions proportional to V_s, which contain the sum of the contribution of both types of spin states and may be compared with the theory of excitation induced dephasing presented in Refs. 43–45. The second one is the bound biexcitonic contribution, which directly couples the orthogonal spin states. Both types of couplings give rise to a strong dependence of FWM signals on the polarization of the external pulses. From phase-space and static interaction contributions, polarization dependencies result from simultaneous excitation of light and heavy holes only.

If we restrict ourselves to the hh contributions, the coupled set of Eqs. (2.10) and (2.14) together with (2.18) can be further simplified and can be reduced to

$$\left(-i\frac{\partial}{\partial t}-i\gamma-\varepsilon_0\right)P=-\boldsymbol{\mu}\mathbf{E}\tilde{\phi}(0)+2b\boldsymbol{\mu}\mathbf{E}|P|^2+VP|P|^2-V_sP(|P|^2+|\tilde{P}|^2)+V_BB\tilde{P}^x, \quad (3.1)$$

where we have lumped the static exciton-exciton interaction and the exchange-type contributions to excitation induced dephasing into a single parameter $V=V_{\text{st}}+V_{\text{exc}}$. Bound biexcitons are described by

$$\left(-i\frac{\partial}{\partial t}-i\gamma_B-\varepsilon_B\right)B=P\tilde{P}. \quad (3.2)$$

P,μ corresponds to the $|3/2h\rangle\rightarrow|1/2e\rangle$ and $\tilde{P},\tilde{\mu}$ to the $|-3/2h\rangle\rightarrow|-1/2e\rangle$ transition, which results from (2.18) by interchanging P with $\tilde{P}$ and μ with $\tilde{\mu}$, respectively. Furthermore, we have introduced a phenomenological dephasing rate γ_B of the biexciton bound state. It is worthwhile to mention that this model, which results from microscopic theory can by no means mapped onto the phenomenological four-level models introduced and evaluated, e.g., in Refs. 17, 62–64. The essential difference is due to the way in which bound biexciton states enter the theory. As can be seen from (3.2), the bound biexciton is not driven by the combined action of an external field and a polarization, but rather by the action of two polarizations. This is an immediate consequence of the existence of a biexcitonic continuum, which leads to the occurrence of the other excitonic correlations contributing to (3.1). The model defined by (3.1) and (3.2) or the corresponding multiband version (2.10) with (2.18) and (2.16) is best suited to explain, at least qualitatively, most experimental results concerning TI-, TR-, and SR-FWM signals for excitation in the vicinity of the excitonic resonance on the same footing. Moreover, it allows us to calculate the various parameters from microscopic theory.

The FWM signal δP resulting from the action of the two pulses E_1 and E_2 in direction $2\mathbf{k}_2-\mathbf{k}_1$ is obtained from (3.1) and (3.2), by means of the usual Fourier decomposition, with respect to the direction of the transmitted signals and the restriction to resonant contributions only. In the present $\chi^{(3)}$ approximation, we obtain

$$\left(-i\frac{\partial}{\partial t}-i\gamma-\varepsilon_0\right)\delta P=+2b\boldsymbol{\mu}\mathbf{E}_2P_2P_1^*+VP_2P_2P_1^*-V_sP_2(P_2P_1^*+\tilde{P}_2\tilde{P}_1^*)+V_BB_{22}\tilde{P}_1^*, \quad (3.3)$$

with

$$\left(-i\frac{\partial}{\partial t}-i\gamma_B-\varepsilon_B\right)B_{22}=P_2\tilde{P}_2. \quad (3.4)$$

P_1 and P_2 are the linear polarizations induced by the fields E_1 and E_2, respectively, and correspondingly for $\tilde{P}_1$ and $\tilde{P}_2$. In this configuration, the maximum of E_2 occurs at $t=0$, whereas the maximum of E_1 is delayed. The influence of the

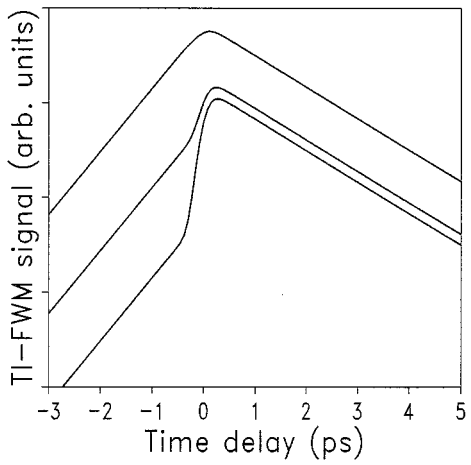

FIG. 3. TI-FWM signals for different ratios of phase-space filling and interaction parameters: $V/b=0.5$ meV, 0.15 meV, 0.05 meV (top to bottom), $\gamma=0.3$ meV. Other parameters are set to zero.

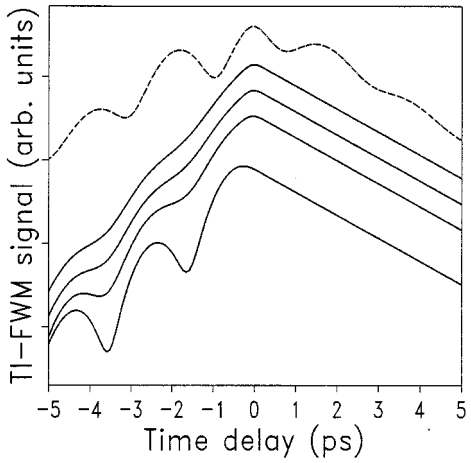

FIG. 4. TI-FWM signals for different values of the screening parameter V_s and collinear polarization: $V_s=20$ meV, 10 meV, 5 meV, 0 (top to bottom). The other parameters are $b=1$, $V=5$ meV, $V_B=5$ meV, $\varepsilon_B=2$ meV, $\gamma_B=\gamma=0.3$ meV. The dashed curve includes $\chi^{(5)}$ contributions for the cross-linear polarized case.

different contributions on FWM signals and their characteristic signatures are illustrated in the following by some numerical results for which we have used parameters appropriate for a GaAs quantum well, assuming an exciton binding energy of 8 meV. The pulse duration is chosen to be 200 fs.

We consider at first the case in which both beams have the same circular polarization and either P or $\tilde{P}$ vanish. Correspondingly, biexcitonic contributions are missing in this configuration and the other interactions contribute in the same way. Thus, the properties of the signal are determined by the ratio of the phase-space filling parameter times Rabi-frequency and an effective interaction parameter. In Fig. 3, the calculated TI-FWM signals are shown for three different ratios of phase-space filling and interaction parameter. If phase-space filling is dominant for small negative time delays, the rising edge of the signal follows the pulse as is expected for a noninteracting two-level system. Only for large time delays does the interaction induced signal contributes to negative time delay with the well-known rising rate 4γ.[30] With increasing interaction parameter, the interaction induced signal becomes dominant. Already for a ratio of 0.5 meV, the step in the signal for negative time delays vanishes and the characteristic shape of the signal is determined by the interaction effects. In real systems, the contributions due to interaction effects are typically several orders of magnitude larger than the phase-space filling contributions and thus dominate the signal completely. For inhomogeneous broadened transitions, however, the contribution for negative time delays vanishes due to interference effects.[65] Nevertheless the absolute magnitude of the signal is determined by the interaction parameters. Phase-space filling effects become more important for high densities or if the detuning is large in comparison with the binding energy.[66] In both cases, however, the present model is not valid.

If we consider the case of linear polarizations of both beams, the biexcitonic contributions come into play for parallel, as well as for orthogonal polarization. In the case of parallel linear polarization, we have in (3.4) $P_2P_1^*=\tilde{P}_2\tilde{P}_1^*$ and the biexcitons contribute only on the background of the excitonic screening contribution. In contrast, choosing orthogonal linear polarization, we have $P_2P_1^*=-\tilde{P}_2\tilde{P}_1^*$. The excitonic screening and thus the dominant contribution to excitation induced dephasing vanishes. As a consequence, biexcitonic contributions become dominant. As in the orthogonal linear geometry, the biexcitonic contribution in (3.3) changes sign, too; this dominance becomes further enhanced.

At first we illustrate the influence of excitonic screening in Fig. 4, where we have varied the magnitude of the parameter V_s for the case of collinear polarization. One of the unique signatures for the contribution of biexcitons, i.e., the beating of the signal, due to the interference of free excitonic transitions with biexcitonic bound state,[59,63,64] is extremely weak as long as excitonic screening contributes. Only if this interaction vanishes the beating evolves into a dominant feature. Thus, orthogonal linear polarization seems to be the configuration best suited to study biexcitonic features experimentally.

A further interesting feature shown in Fig. 4 is the missing of beats for positive time delays. This is an immediate consequence of the $\chi^{(3)}$ approximation, in which—considering the $2\mathbf{k}_2-\mathbf{k}_1$ direction—only bound biexciton states excited by the second pulse contribute. This is no longer valid if higher order contributions are taken into account. Although we will not extend our discussion to a complete analysis of the $\chi^{(5)}$-approximation scheme, the most important features should be mentioned. If we extend the validity of Eq. (2.5) up to the fifth order in the field, there occurs a rich variety of additional contributions, most of which, however, do not influence the qualitative features of the generalized nonlinear Schrödinger equation. Apart from excitation induced dephasing processes, which on $\chi^{(5)}$ level yield an increase of the dephasing rates, the most important $\chi^{(5)}$ contribution, entering (3.1) is proportional to B^*PPP. Further, already without the explicit fifth-order contributions (3.1) contains, implicitely $\chi^{(5)}$ contributions to the FWM signal, if we allow for nonlinear contributions to P on the right-hand side. As a consequence of the additional contributions,

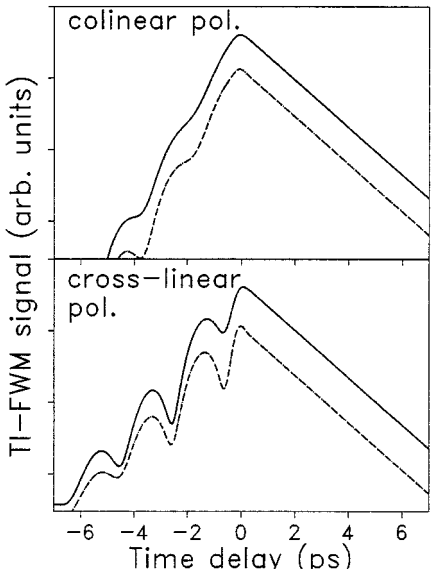

FIG. 5. TI-FWM signals for collinear and cross-linear polarization. Full lines correspond to resonant exciton excitation, dashed lines to resonant biexciton excitation. The screening parameter is $V_s=10$ meV, other parameters are the same as in Fig. 4.

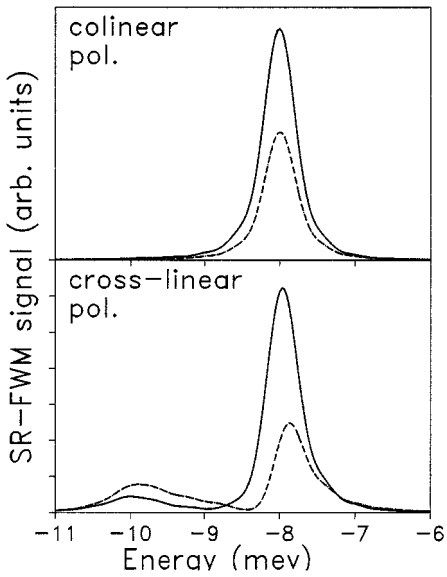

FIG. 6. SR-FWM signals for collinear and cross-linear polarization. Full lines correspond to resonant exciton excitation, dashed lines to resonant biexciton excitation. The screening parameter is $V_s=10$ meV, other parameters are the same as in Fig. 4.

the excitation of the biexciton by E_1 also influences the FWM signal in $2\mathbf{k}_2-\mathbf{k}_1$ direction. This process yields beats also for positive time delays, as is shown for cross-linear polarization in Fig. 4. In contrast to the collinear polarized geometry, the rise time of the signal for negative time delay has become slower and the typical asymmetric shape of the signal is disturbed (compare Fig. 3). This behavior depends sensitively on the ratio of excitonic and biexcitonic dephasing rates and occurs already within the $\chi^{(3)}$ approximation. The switch of this asymmetry of the TI-FWM signal (compare Fig. 3) has been found experimentally already, e.g., in Ref. 16. As can be recognized in Fig. 5, for $\gamma_B=\gamma$ in the collinear polarized case, the rise time of the signal is determined by the excitonic dephasing time, whereas in the cross-linear case the biexcitonic dephasing becomes dominant. Considering δ pulses it can be easily shown analytically, that the slower rise time of the signal for cross-linear polarization is present, as long as the dephasing rate of the biexciton obeys the condition $\gamma_B<2\gamma$. As was confirmed only recently, by experimental data in Ref. 64 this condition is indeed fulfilled.

Tuning the central frequency of the pulse from the excitonic to the biexcitonic resonance leads to a further decrease of the rise time. This effect, however, is rather weak, as long as the spectral width of the pulse is large in comparison with the biexcitonic binding energy. In the opposite limit (not shown), the decrease of the rise time occurs only if the pulse is in resonance with the biexciton. This is again in agreement with recent experimental results[16,64] and confirmed by our experimental data. It should be noted, however, that the interpretation of this behavior in terms of a reversal of the time axis of the biexcitonic signal is misleading. In the case of spectrally narrow resonant excitation of the biexciton, the slope of the signal for negative time delays is unambigously given by $2\gamma_B$. Thus, the asymmetry of the signal is determined by the ratio of excitonic and biexcitonic dephasing rates.

In real systems, there are several effects which can mask the signatures of biexcitonic contributions discussed in this section. In the case of ultrashort excitation, the large spectral width of the pulse prevents the excitation of hh excitons solely and lh excitons are also excited. The simultaneous excitation of hh and lh excitons yields, in the FWM signals pronounced quantum beats, which cover the exciton-biexciton beats. Dephasing times shorter than those used in the calculations can additionally hinder an experimental resolution of exciton-biexciton beating. In this case, biexcitons can show up in TR-FWM signals only via a reduced rise time of the signal for cross-linear polarization. An additional confirmation for the occurrence of biexcitons can be given by considering the spectrally resolved signals.

In Fig. 6, SR-FWM signals are shown again for collinear and cross-linear polarization. Whereas in the collinear case only the excitonic resonance is present, the biexcitonic resonance shows up as pronounced peak in the cross-linear case. As expected, this contribution is further enhanced by resonant excitation of the biexciton. Considering corresponding TR-FWM signals one obtains the same behavior, which has been demonstrated several times already on the basis of the SBE's.[29] For positive time delay, the bulk of the signal is always delayed. The delay, however, is not correlated with the delay between the pulses, but roughly determined by the dephasing time. On the considered excitation conditions, the phase-space filling, which leads to an instantaneous contribution to the TR-FWM signal, is completely negligible (for a detailed study of this contribution compare, e.g., Refs. 66, 67). Apart from exciton-biexciton quantum beats, the biexcitonic contributions give also rise to an interaction induced signal and have thus the same consequences as the other

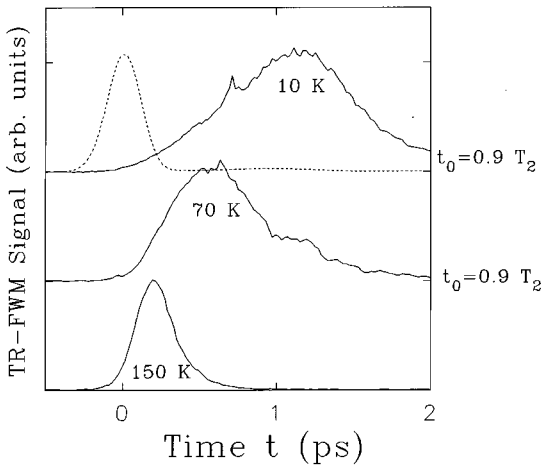

FIG. 7. Temperature dependence of TR-FWM from sample A at $T=1$ ps in the collinearly polarized geometry. Temperatures are from top to bottom: 10, 70, and 150 K. The relationships between the peak positions T_0 and T_2, determined from TI-FWM, are written on the right sides for 10 and 70 K. The density is estimated to be 10^{10} cm^{-2}. The broken lines denote the transmitted pulse shape.

interaction contributions. This will be demonstrated in the following by experimental results, which represent a systematic study of the discussed interaction effects.

IV. SAMPLES AND EXPERIMENTAL CONDITIONS

In the TI-, TR-, and SR-FWM experiments described in Fig. 1(a), three GaAs quantum well samples with their substrates removed were investigated. Two samples have absorption widths at the heavy-hole exciton, which are less than 1 meV and have a well width of 17 nm (sample A: 10 wells, absorption width 0.7 meV; sample B: 15 wells, absorption width 0.9 meV). Both samples A and B have negligible Stokes shift between photoluminescence and photoluminescence excitation spectra, and pulse distortions are minimal. We have also used an optically thick, inhomogeneously broadened sample (sample C: 10 nm, 65 wells, absorption width 4 meV) with non-negligible pulse distortion. Due to inhomogeneous broadening, a strong photon echo is expected for TR-FWM from sample C, in agreement with experimental and theoretical results in Ref. 65. These three samples A, B, and C, in cross and collinearly polarized geometries, provide us with ideal situations to investigate the time evolution of FWM originating from excitons, biexcitons, and bound excitons. The laser used in our various FWM experiments [compare Fig. 1(a)] was a widely tunable, self-mode-locked Ti-sapphire laser that produces transform limited pulses of 100–200 fs (10–20-meV bandwidths). In TI- and especially in TR-FWM experiments, the proper determination of zero delays $T=0$ and $t=0$ is very important for the interpretation of the experimental results. We determined $T=0$ by looking at TI-FWM signals in both phase matched directions $2\mathbf{k}_2-\mathbf{k}_1$ and $2\mathbf{k}_1-\mathbf{k}_2$ and by utilizing time reversal symmetry. In TR-FWM, the arrival of beam 1 and beam 2 ($t=0$) on the sample was measured within 20 fs by upconverting the scattered light of beams 1 and 2 into the direction of the phase-matched direction.

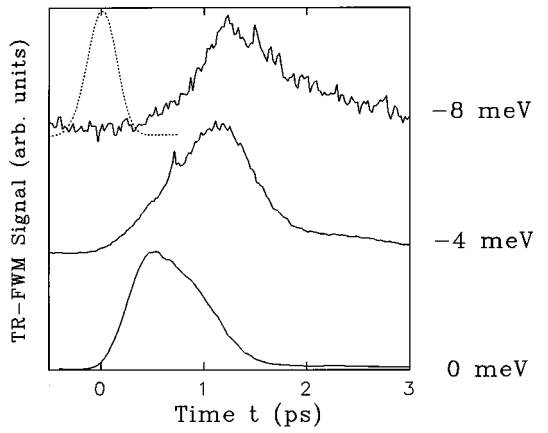

FIG. 8. TR-FWM in the collinearly polarized geometry from sample A at 10 K and $T=1$ ps at three different detunings: -8, -4, and 0 meV (from top to bottom). The density for the -4 meV detuning is estimated to be 10^{10} cm^{-2}. The upconverted pulse shape is represented by broken lines.

V. TR- AND SR-FWM OF HIGH-QUALITY SAMPLES OBTAINED WITH COLLINEARLY POLARIZED BEAMS

We now turn to TR-FWM and SR-FWM experiments with collinearly polarized beams on samples A and B. The purpose of TR-FWM experiments on these samples is to demonstrate that the diffraction of interaction induced fields is the dominant source of FWM signals. Independent of the microscopic origin of the induced fields, the signature of this dominance is a delayed signal. The phase-space contribution, which gives rise to an instantaneous signal, is completely missing and would become significant only at high densities or at large detuning.[66]

In Fig. 2(a), we have observed the long rise time of the TR-FWM signal, where the signal continues to rise long after both beams passed through. To determine the relationship of the delay to the macroscopic dephasing time T_2, the temperature dependence of the TR-FWM at $T=1$ ps was measured, as shown in Fig. 7. The peak of the TR-FWM moves closer to $t=0$ as the temperature increases and occurs roughly at T_2, measured by TI-FWM. The same decay rate is approached also by the asymptotic behavior of the corresponding TR-FWM signal.

As the dephasing rate of excitons depends sensitively on the density of free carriers, which are simultaneously excited, we can further vary T_2 by varying the detuning. In Fig. 8, TR-FWM at $T=1$ ps and 10 K at three different detunings are displayed. As expected, the peak position of TR-FWM shifts closer to $t=0$ with decreasing detuning, because T_2 decreases with increasing density of free carriers, due to exciton-free carrier interaction. The peak occurs again near T_2, as determined by TI- and TR-FWM.

Investigating now the intensity dependence of TR-FWM from sample B at 10 K at a detuning of $+4$ meV, shown in Fig. 9, we see that at low density (top: 3×10^9 cm^{-2}), the peak is delayed and hh-lh quantum beats are clearly visible, due to the simultaneous excitation of lh excitons and hh excitons. As the density becomes higher (bottom: 3×10^{10}

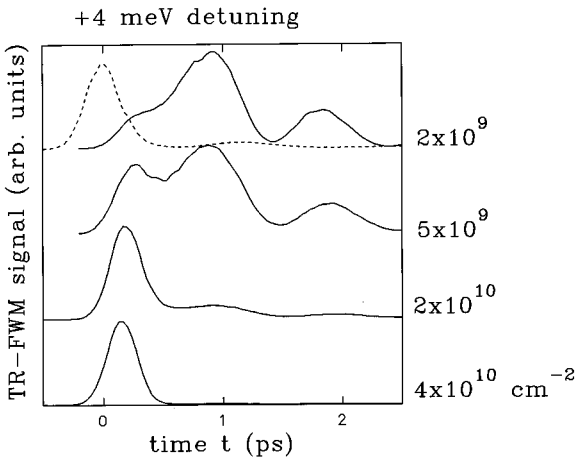

FIG. 9. Intensity dependence of TR-FWM from sample *B* at 10 K, $T=1$ ps, at +4 meV detuning from the hh. The densities are estimated to be 2×10^9 cm^{-2} (top) and 3×10^{10} cm^{-2} (bottom).

cm^{-2}), T_2 becomes much shorter and the peak position is shifted again closer to $t=0$.

The results discussed thus far demonstrate that in both samples *A* and *B*, TR-FWM is characterized by a single maximum close to T_2, which we have varied over a wide range by varying temperature, density, and detuning. Therefore, we can immediately conclude that in both samples, the diffraction of induced fields completely dominates the diffraction of external fields, which would result in a peak at $t=0.1$–0.2 ps. Noninteracting few level models, which assume the dominance of the external fields, are thus completely inadequate for describing the nonlinear optics of semiconductors. Figures 7 and 8 illustrate that the diffraction of the interaction induced field still dominates for T_2 as small as 0.5 ps. Up to this point, the peak of TR-FWM is completely separated from the pulse.

We now examine whether the dominance of the diffraction of the induced field is affected by going further to lower densities. In order to verify that the interaction induced fields dominate also in the low-density limit, we have performed TR-FWM at 50 K on sample *B* at a detuning of −4 meV, where T_2 is primarily determined by exciton-phonon interaction (Fig. 10). Varying the density over nearly two orders of magnitude, the position of the peak in TR-FWM remains well delayed. Also the existence of a signal at negative time delays and the relative strength of it (relative to the positive time delay signal) does not change in TI-FWM experiments, as the density is further lowered (10^7 cm^{-2}, not shown). These results demonstrate that, in the low-density limit, the interaction induced field becomes a density independent source of FWM signals, in accordance with the theory.

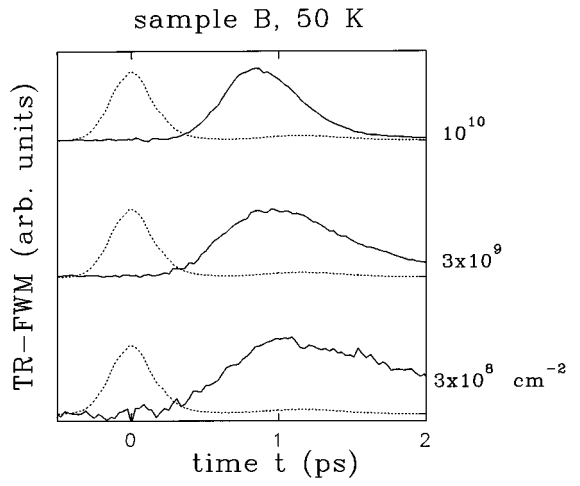

FIG. 10. Density dependence of TR-FWM from sample *B* at $T=1$ ps and 50 K at a detuning of −4 meV from the hh. The densities are (from top to bottom): 10^{10} cm^{-2}, 3×10^9 cm^{-2}, and 3×10^8 cm^{-2}. The transmitted pulse shape is represented by broken lines.

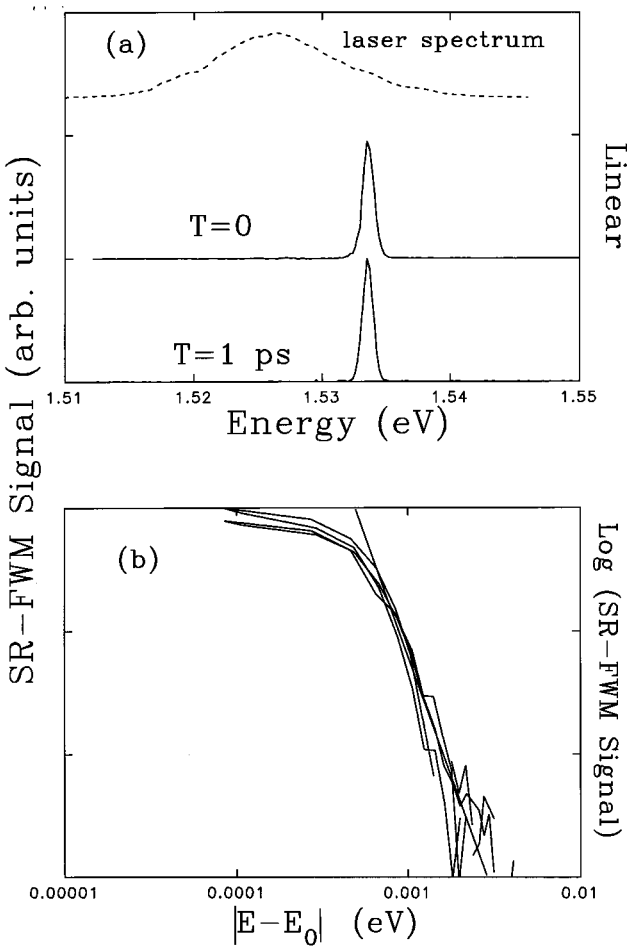

FIG. 11. (a) SR-FWM from sample *A* at 10 K and $T=0$ (top) and 1 ps (bottom). The density is relatively low (2×10^9 cm^{-2}). The broken lines denote the laser spectrum. (b) Log-log plot of the SR-FWM data of Fig. 12(a) versus the absolute detuning. The broken lines, a guide to the eyes, have a slope of 3.9.

Thus far, our discussion was centered on the time domain. It is instructive to spectrally resolve the diffracted signal, in order to classify the microscopic origin of the induced field. In Fig. 11(a), such SR-FWM spectra from sample *A* are shown at time delays 0 and 1 ps at 5×10^9 cm^{-2}. The spectrum is completely dominated by the $1s$-exciton peak. The log-log plot of the SR-FWM data presented in Fig. 11(a) is shown in Fig. 11(b). It indicates that the high-energy tail of the peak has slope close to 4. This is consistent with even the

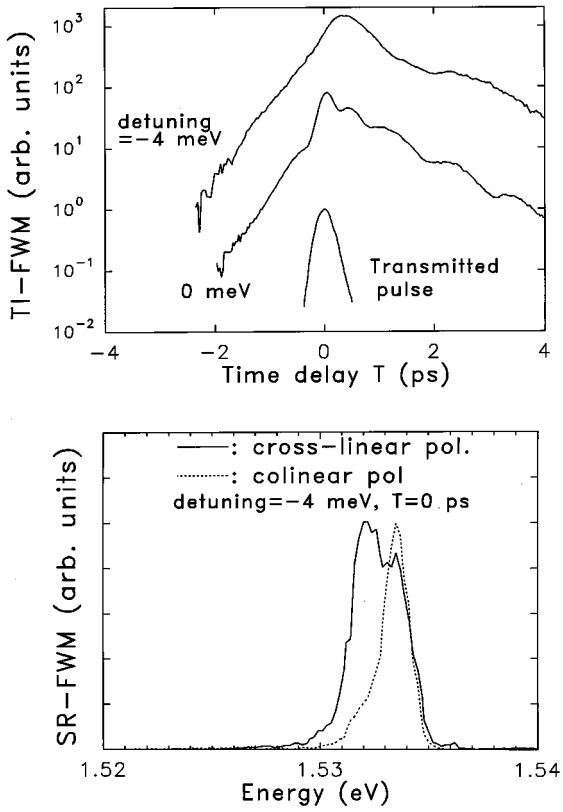

FIG. 12. (a) TI-FWM from sample A at 10 K in the cross linearly polarized geometry at detunings of 4 meV (top) and 0 meV (middle) from the hh resonance. At the bottom, the transmitted pulse shape determined by the cross correlation in a nonlinear crystal is shown. (b) SR-FWM for the cross and collinear polarization geometries at zero delay. The density is estimated to be 10^{10} cm^{-2}.

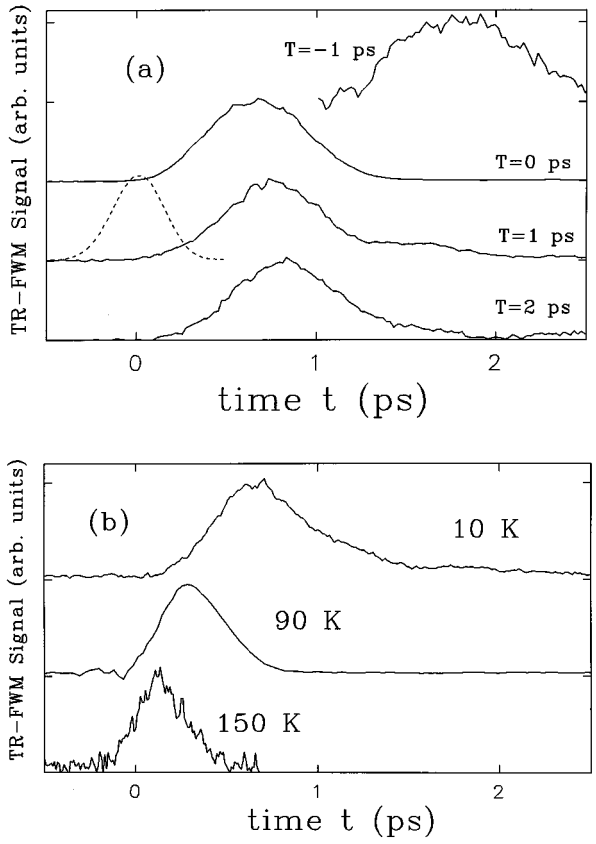

FIG. 13. (a) TR-FWM from sample A at 10 K obtained with cross linearly polarized beams, at a detuning of -4 meV from the hh. The time delays are from top to bottom, -1, 0, 1, and 2 ps. The density is estimated to be 10^{10} cm^{-2} and the broken lines represent the autocorrelated pulse shape after transmission. (b) Temperature dependence of TR-FWM from sample A at the cross linearly polarized geometry; temperatures are, from top to bottom 10, 90, 150 K.

simplest picture of interaction induced signals, which results immediately from Eq. (3.3), considering excitation with δ pulses. For zero delay and neglecting phase-space filling, the signal is proportional to $\theta(t)[1-\exp(-t/T_2)]\exp(-t/2T_2)$.[20] Fourier-transforming $\delta P(t)$, one finds that the asymptotic behavior of the corresponding SR-FWM signal $|\delta P(\omega)|^2$ is proportional to $(\omega-\omega_0)^4$. This is indeed not far from our experimental data. The dotted line, which is a guide to the eyes, has a slope of 3.9.

VI. TR- AND SR-FWM WITH CROSS LINEARLY POLARIZED BEAMS

In the previous section, we discussed TR-FWM and SR-FWM experiments with collinearly polarized beams. In this section, we discuss the time evolution of FWM, where biexcitons or bound excitons give rise to dominant contributions. At first we discuss TI-, SR-, and TR-FWM from sample A, where bound excitons make significant contribution. In Fig. 12(a), TI-FWM at 10 K from sample A in the cross linearly polarized geometry at 10 K for detunings of -4 meV (top) and 0 meV (middle) measured from the hh exciton resonance are shown, along with the transmitted pulse shape (bottom). The decay constants for $T<0$ are definitely smaller than those for $T>0$, by more than a factor of 2. Furthermore, SR-FWM at $T=0$ shown in Fig 12(b) displays a strong peak roughly 1.5 meV below the hh exciton. For $T>0$, this peak remains strong, whereas for $T<0$, it is much weaker but not negligible. In an earlier work on the same sample, this peak could be assigned to a bound excitonic contribution by analyzing TI-FWM, as well as the intensity dependence of cw luminescence.[68]

Figure 13(a) shows TR-FWM from sample A at $T=-1$, 0, 1, and 2 ps under nearly identical conditions as in Fig. 12(b). The density is estimated to be 10^{10} cm^{-2}. At $T=-1$ ps, SR-FWM is dominated by the excitonic contribution (not shown), whereas at $T=0$, 1, and 2 ps, bound excitonic contribution as shown in Fig. 12(b) are very strong. The pulse shape and position of the second beam are indicated by broken lines. Again, TR-FWM signals are well delayed, peaking at about 0.7 ps after the arrival of the second beam. From these observations, we can conclude that also TR-FWM from bound excitons is dominated by the diffraction of the interaction induced field. The temperature dependence of TR-FWM is shown in Fig. 13(b). As in the case of collinear polarization, the peak position shifts closer to $t=0$ with increasing temperature, but remains well separated from the pulse.

In Fig. 14(a), TI-FWM from samples B in the cross linearly polarized geometry are plotted at exciton densities 10^{10}

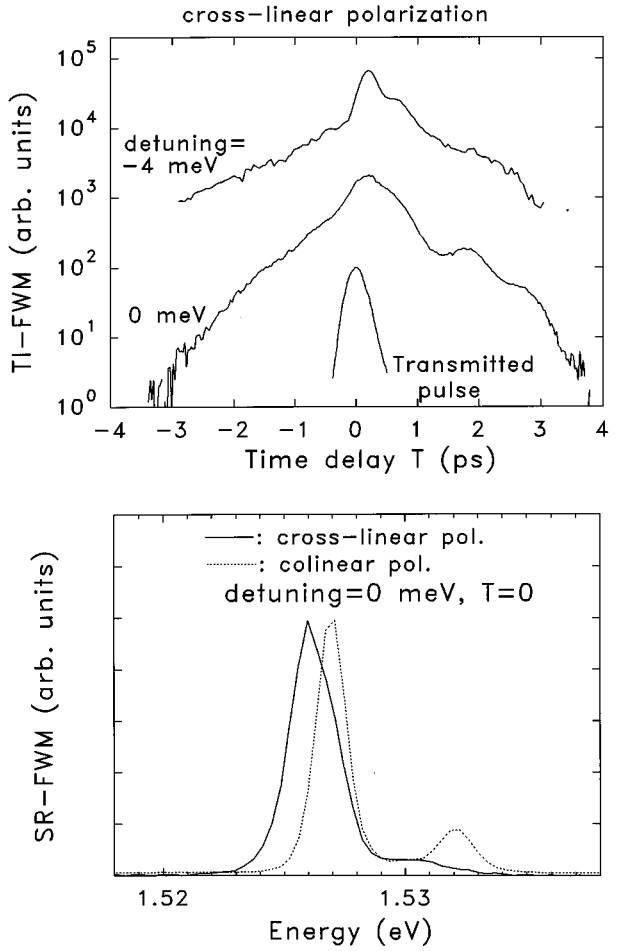

FIG. 14. (a) TI-FWM from sample *B* at 10 K in the cross linearly polarized geometry at detunings of −4 meV (top) and 0 meV (middle) from the hh resonance. At the bottom, the transmitted pulse shape determined by the cross correlation in a nonlinear crystal is shown. (b) SR-FWM for the cross and the collinear polarization at $T=0$ ps.

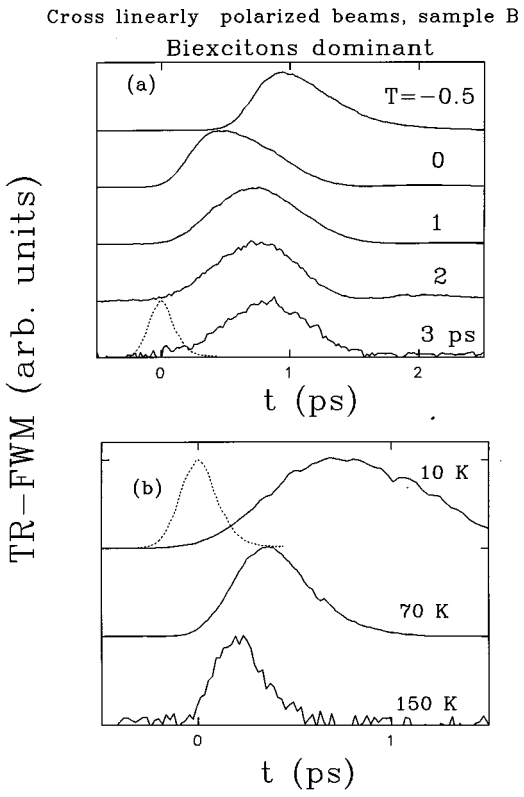

FIG. 15. (a) TR-FWM from sample *B* under nearly identical conditions as Fig. 13. Time delays are from top to bottom −0.5, 0, and 1 ps. The temperatures are, from top to bottom, 10, 70, and 150 K. Broken lines represent the shape and positions of the second beam arriving at the sample.

cm^{-2} and 10 K. The laser is tuned 4 meV below the heavy-hole (hh) exciton (top), or at resonance with hh exciton (middle). At the bottom, the cross correlated pulse shape after transmission is shown. For negative time delay, the rise time of the signal becomes considerably slower when the detuning is decreased. Considering our theoretical analysis, this suggests the existence of a resonance below the 1*s* exciton, with different dephasing time. SR-FWM shown in Fig. 14(b) for zero delay, 10 K and vanishing detuning confirms this interpretation. In the cross-linear configuration, we obtain a peak roughly 1 meV below the excitonic resonance, which can be attributed to a bound biexciton. The corresponding TI-FWM signals demonstrate clearly that the dephasing rate γ_B of biexcitons is considerably smaller than 2γ (compare the discussion in Sec. III), in agreement with results in Ref. 64. The lh excitonic contribution is also shown, roughly 5 meV above the hh. The biexcitonic contribution in the cross linearly polarized geometry remains strong for both the negative and the positive time delays, as determined by SR-FWM. Further, TI- and SR-FWM studies on this sample, using circularly as well as linearly polarized beams, confirm that this peak indeed results from a biexcitonic contribution to FWM. TR-FWM on sample *B* in the cross linearly polarized geometry exhibits again the signature of interaction induced fields, which now result mainly from exciton-biexciton interaction.

In Fig. 15(a), the results of TR-FWM on sample *B* under conditions comparable with Figs. 14(a) and 14(b) are shown at various time delays. The peaks occur well away from the passage of beam 2 at $t=0$ or that of beam 1, which occurs at $t=0.5$, 0, −1, −2, −3 ps for $T=0.5$, 0, 1, 2, 3 ps, respectively. The positions and pulse shapes of the second beam determined by cross correlation are denoted by broken lines. Considering the temperature dependence of TR-FWM shown in Fig. 15(b), we see that as before the peak positions in Fig. 15(b) shifts closer to $t=0$ as temperature and correspondingly the dephasing is increased. At higher temperatures, biexcitons dissociate and excitons, not biexcitons should make the dominant contribution. Therefore, it is expected that TR-FWM at 70 and 150 K result mostly from excitons, whereas at 10 K, biexcitons dominate. Nevertheless, in both cases, the signal is delayed.

As we have shown in the theoretical part, electromagnetic fields inside a semiconductor, which result from static and dynamical exciton-exciton interaction, as well as from exciton-biexciton interaction, give rise to internal fields, which act as a source of FWM signals. Our experiments demonstrate unambiguously that these interaction induced

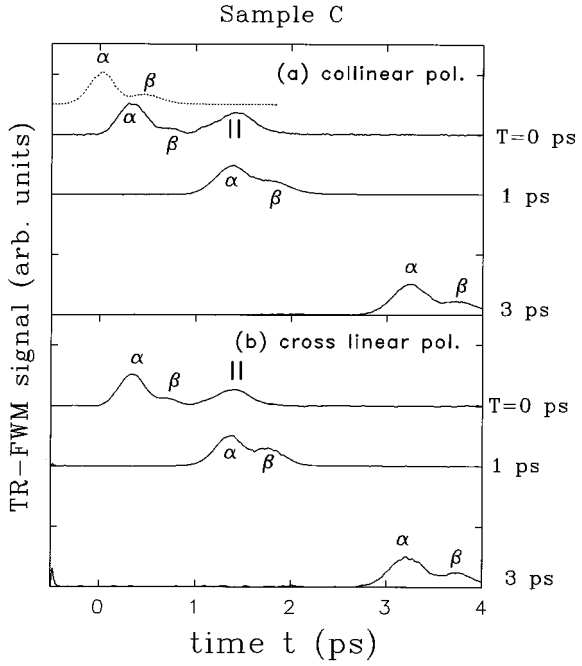

FIG. 16. TR-FWM from sample *C* in (a) the collinearly polarized geometry and (b) the cross linearly polarized geometry. The transmitted pulse shape is represented by broken lines. The detuning is -4 meV and the density is estimated to be 10^9 cm^{-2}.

fields are the dominant source of FWM in semiconductors. There are several possibilities to reduce this dominance. At high-densities interaction induced signals saturate or even start to decrease, due to screening effects. The phase-space contribution, however, increases at least linearly with the external field. Thus, the ratio of interaction induced and phase-space filling contributions of the signal can be inverted at high density. This effect depends sensitively on the screening of interaction induced fields, which increases with increasing density. The relative contribution of interaction induced fields depends, however, not only on the excitation conditions, but also sensitively on the quality of the sample.

VII. TR-FWM OF INHOMOGENEOUSLY BROADENED SAMPLE *C*

In previous sections, we discussed TR-FWM mainly in high-quality samples *A* and *B*, where small inhomogeneous broadenings do not affect the interpretation of the results. In this section, we discuss TR-FWM in inhomogeneously broadened sample *C*, where a strong photon echo is expected.[25,65]

In Figs. 16(a) and 16(b), we show TR-FWM of sample *C* at 10 K and at relatively low density (2×10^9 cm^{-2}), tuned slightly below hh exciton for the crosslinearly [Fig. 16(b)] and the collinearly polarized geometries. The transmitted pulse shape [broken lines, top of Fig. 16(a)] is somewhat distorted, with a secondary peak, which is roughly three times smaller than the primary peak. This is because of the relatively large total thickness (650 nm), which leads to pronounced propagation effects. In both polarization geometries, the signature of a photon echo is obvious: the peak occurs roughly at the delay between both pulses. Furthermore, the distorted pulse shape is reflected in the shape of the echo signals, with peaks α and β readily identifiable.

At $T=0$, an additional peak at 1.4 ps occurs in both polarizations geometries. Since at this time both pulses have completely passed through the sample, we can identify this peak as an interaction induced signal. The instantaneous signal near $t=0$ is due to diffraction of the external field, i.e., the phase-space filling contribution. At a delay of $T=1$ ps, the position of the interaction induced signal coincides with the echo like contribution, whereas at $T=3$ ps, the interaction induced signal becomes completely negligible. The separate occurence of an instantaneous and an interaction induced contribution at zero delay is in contrast to the results in Ref. 65, and can be attributed to the long dephasing time of roughly 1.5 ps. The increase of the temporal duration of the echo with increasing delay, which results from the Coulomb interaction is rather weak due to the strong inhomogeneous broadening.

Echolike behavior results also in homogeneous systems for excitation of the excitonic continuum, which acts similar as inhomogeneous broadening of discrete energy levels.[31] In the worst case, FWM signals are determined by combined effects, due interaction induced fields, inhomogeneous broadening and continuum excitation, which in thick samples are further influenced by propagation effects. The result is a complex temporal evolution, which in many cases allows no simple interpretation, but requires a careful theoretical analysis.

VIII. SUMMARY AND CONCLUSIONS

To summarize our results, we have shown that FWM experiments are completely dominated by interaction induced fields when the laser spectrum encompasses excitonic resonances. We have developed a unified theoretical approach that includes static and dynamical exciton-exciton interaction, as well as exciton-biexciton interaction. These interaction processes induce internal fields, which lead to pronounced contribution to FWM signals. Assuming resonant excitation conditions, we have shown that the resulting model is best suited to explain the properties of FWM signals, especially their dependence on the polarization geometry.

Our experimental data show unambigously that the interaction induced fields dominate FWM signals completely. Regardless of the microscopic origin (excitons, bound excitons, or biexcitons) of the induced fields, the TR-FWM signal is always delayed. No instantaneous signal contributes, which allows the conclusion that the phase-space contribution and thus the self-diffraction of external fields is negligible in comparison with the fields induced by many-particle interactions.

ACKNOWLEDGMENTS

This work (D.S.K.) was partially supported by the Korean Science and Engineering Foundation. The experimental work of D.S.K. was done while he was with AT&T Bell Laboratories, Holmdel.

[1] H. J. Eichler, P. Günther, and D. W. Pohl, *Laser-Induced Dynamical Grating* (Springer Verlag, Berlin, 1980).
[2] B. S. Wherrett, A. L. Smirl, and T. F. Bogess, IEEE J. Quantum Electron. **QE-19**, 680 (1983).
[3] L. Schultheis, J. Kuhl, A. Honold, and C. W. Tu, Phys. Rev. Lett. **57**, 1635 (1986); **57**, 1797 (1986).
[4] P. C. Becker, H. L. Fragnito, C. H. Brito Cruz, R. L. Fork, J. E. Cunningham, J. E. Henry, and C. V. Shank, Phys. Rev. Lett. **61**, 1647 (1988).
[5] A. Honold, L. Schultheis, J. Kuhl, and C. W. Tu, Appl. Phys. Lett. **52**, 2105 (1988).
[6] L. Schultheis, A. Honold, J. Kuhl, and C. W. Tu, Phys. Rev. B **40**, 6442 (1989).
[7] C. Dörnfeld and J. H. Hvam, IEEE J. Quantum Electron. **QE-25**, 904 (1989).
[8] K. Leo, T. C. Damen, J. Shah, and K. Köhler, Phys. Rev. B **42**, 11 359 (1990).
[9] A. Honold, T. Saku, Y. Horikoshi, and K. Köhler, Phys. Rev. B **45**, 6010 (1992).
[10] J. Y. Bigot, M. T. Portella, R. W. Schoenlein, J. E. Cunningham, J. E. Henry, and C. V. Shank, Phys. Rev. Lett. **67**, 636 (1991).
[11] S. T. Cundiff, H. Wang, and D. G. Steel, Phys. Rev. B **46**, 7248 (1992).
[12] D. S. Kim, J. Shah, J. E. Cunningham, T. C. Damen, W. Schäfer, M. Hartmann, and S. Schmitt-Rink, Phys. Rev. Lett. **68**, 1006 (1992); **68**, 2838 (1992).
[13] R. Raj, I. Abram, and J. A. Levenson, Solid State Commun. **81**, 51 (1992).
[14] R. T. Phillips, D. J. Lovering, G. J. Denton, and G. W. Smith, Phys. Rev. B **45**, 4308 (1992).
[15] D. Lovering, R. T. Phillips, and G. J. Denton, Phys. Rev. Lett. **68**, 1880 (1992).
[16] B. F. Feuerbacher, J. Kuhl, and K. Ploog, Phys. Rev. B **43**, 2439 (1991).
[17] G. Finkelstein, S. Bar-Ad, and I. Bar-Joseph, Phys. Rev. B **47**, 12 964 (1993).
[18] T. Yajima and T. Taira, J. Phys. Soc. Jpn. **47**, 1620 (1979).
[19] I. Abram, Phys. Rev. B **40**, 5460 (1989).
[20] M. Wegener, D. S. Chemla, S. Schmitt-Rink, and W. Schäfer, Phys. Rev. A **42**, 5675 (1990).
[21] K. Leo, J. Shah, E. O. Göbel, T. C. Damen, S. Schmitt-Rink, W. Schäfer, and K. Köhler, Phys. Rev. Lett. **66**, 934 (1991).
[22] K. Leo, M. Wegener, J. Shah, D. S. Chemla, E. O. Göbel, T. C. Damen, S. Schmitt-Rink, and W. Schäfer, Phys. Rev. Lett. **65**, 1340 (1990).
[23] K. Leo, E. O. Göbel, T. C. Damen, J. Shah, S. Schmitt-Rink, W. Schäfer, J. E. Müller, K. Köhler, and P. Ganser, Phys. Rev. B **44**, 5726 (1991).
[24] D. S. Kim, J. Shah, T. C. Damen, W. Schäfer, F. Jahnke, S. Schmitt-Rink, and K. Köhler, Phys. Rev. Lett. **69**, 2725 (1992).
[25] M. D. Webb, S. T. Cundiff, and D. G. Steel, Phys. Rev. Lett. **66**, 934 (1991); **69**, 2685 (1992).
[26] S. Weiss, M.-A. Mycek, J.-Y. Bigot, S. Schmitt-Rink, and D. S. Chemla, Phys. Rev. Lett. **69**, 2685 (1992).
[27] A. Stahl and I. Balslev, *Electrodynamics of the Semiconductor Band-Edge*, Springer Tracts in Modern Physics Vol. 110 (Springer, Berlin, 1986).
[28] H. Haug and S. W. Koch, *Quantum Theory of the Optical and Electronic Properties of Semiconductors* (World Scientific, Singapore, 1990).
[29] W. Schäfer, in *Optics of Semiconductor Nanostructures*, edited by F. Henneberger, S. Schmitt-Rink and E. O. Göbel (Akademie Verlag, Berlin, 1993), and references therein.
[30] C. Stafford, S. Schmitt-Rink, and W. Schäfer, Phys. Rev. B **41**, 10 000 (1990).
[31] M. Lindberg, R. Binder, and S. W. Koch, Phys. Rev. A **45**, 1865 (1992).
[32] S. W. Koch, A. Knorr, R. Binder, and M. Lindberg, Phys. Status Solidi B **173**, 177 (1992).
[33] W. Schäfer, F. Jahnke, and S. Schmitt-Rink, Phys. Rev. B **47**, 1217 (1993).
[34] D. Fröhlich, A. Kuhlik, B. Uebbing, A. Mysyrowicz, V. Langer, H. Stolz, and W. von der Osten, Phys. Rev. Lett. **67**, 2343 (1991).
[35] T. Rappen, G. Mohs, and M. Wegener, Phys. Status Solidi B **173**, 77 (1992).
[36] H. Stolz, Phys. Status Solidi **173**, 99 (1992).
[37] P. Schillak and I. Balslev, Phys. Rev. B **48**, 9426 (1993).
[38] H. J. Bakker and H. Kurz, Phys. Rev. B **50**, 7805 (1994).
[39] A. Schulze, A. Knorr, and S. W. Koch, Phys. Rev. B **51**, 10 601 (1995).
[40] K. H. Pantke P. Schillak, B. S. Razbirin, V. G. Lyssenko, and J. M. Hvam, Phys. Rev. Lett. **70**, 327 (1993).
[41] K. H. Pantke and J. M. Hvam, Int. J. Mod. Phys. B **8**, 73 (1994), and references therein.
[42] H. H. Yaffe, Y. Prior, J. P. Harbison, and L. T. Florenz, J. Opt. Soc. Am. B **10**, 578 (1993).
[43] H. Wang, K. B. Ferrio, D. G. Steel, Y. Z. Hu, R. Binder, and S. W. Koch, Phys. Rev. Lett. **71**, 1261 (1993).
[44] H. Wang, K. B. Ferrio, D. G. Steel, P. R. Berman, Y. Z. Hu, R. Binder, and S. W. Koch, Phys. Rev. A **49**, 1551 (1994).
[45] Y. Z. Hu, R. Binder, S. W. Koch, S. T. Cundiff, H. Wanq, and D. G. Steel, Phys. Rev. B **49**, 14 382 (1994).
[46] T. Rappen, U. G. Peter, M. Wegener, and W. Schäfer, Phys. Rev. B **49**, 7817 (1994).
[47] T. Saiki, M. Kuwata-Gonokami, T. Matsusue, and H. Sakaki, Phys. Rev. B **49**, 7817 (1994).
[48] M. Lindberg, R. Binder, Y. Z. Hu, and S. W. Koch, Phys. Rev. B **49**, 16 942 (1994).
[49] R. Binder and S. W. Koch, Prog. Quantum. Electron. **19**, 307 (1995).
[50] R. Zimmermann, *Many-Particle Theory of Highly Excited Semiconductors* (Teubner, Leibzig, 1987).
[51] V. M. Axt and A. Stahl, Z. Phys. B **93**, 195 (1994).
[52] V. M. Axt and A. Stahl, Z. Phys. B **93**, 205 (1994).
[53] M. Lindberg, Y. Z. Hu, R. Binder, and S. W. Koch, Phys. Rev. B **50**, 18 060 (1994).
[54] R. C. Miller, D. A. Kleinman, A. C. Gossard, and O. Munteanu, Phys. Rev. B **28**, 871 (1983).
[55] E. Hanamura and H. Haug, Phys. Rep. **33**, 210 (1977).
[56] A. Maruani and D. S. Chemla, Phys. Rev. B **23**, 841 (1981).
[57] C. Klingshirn and H. Haug, Phys. Rep. **77**, 315 (1981).
[58] M. Combescot and R. Combescot, Phys. Rev. B **40**, 3788 (1989).
[59] K. H. Pantke, D. Oberhauser, V. G. Lyssenko, J. M. Hvam, and G. Weimann, Phys. Rev. B **47**, 2413 (1993).
[60] F. Kreller, M. Lowisch, J. Puls, and F. Henneberger, Phys. Rev. Lett. **75**, 2420 (1995).
[61] D. S. Chemla, J.-Y. Bigot, M.-A. Mycek, S. Weiss, and W. Schäfer, Phys. Rev. B **50**, 8439 (1994).
[62] K. Bott, O. Heller, D. Bennhardt, S. T. Cundiff, P. Thomas, E. J. Mayer, G. O. Smith, R. Eccleston, and J. Kuhl, Phys. Rev. B **48**, 17 418 (1993).

[63] J. Kuhl, E. J. Mayer, G. Smith, R. Eccleston, D. Bennhardt, P. Thomas, K. Bott, and O. Heller, in *Coherent Optical Interactions in Semiconductors*, Vol. 330 of *NATO Advanced Series B: Physics*, edited by R. T. Phillips (Plenum, New York, 1994), p. 1.
[64] E. J. Mayer *et al.*, Phys. Rev. B **50**, 14 730 (1994).
[65] F. Jahnke *et al.*, Phys. Rev. B **50**, 8114 (1994).
[66] D. S. Kim, J. Shah, T. C. Damen, W. Schäfer, L. Pfeiffer, and K. Köhler, Phys. Rev. B **50**, 15 086 (1994).
[67] P. Leisching, W. Beck, H. Kurz, W. Schäfer, K. Leo, and K. Köhler, Phys. Rev. B **51**, 7962 (1995).
[68] K. Leo, T. C. Damen, J. Shah, and K. Köhler, Phys. Rev. B **42**, 11 359 (1990).